

Theoretical Analysis of the Triplet Excited State of the $[\text{Pt}_2(\text{H}_2\text{P}_2\text{O}_5)_4]^{4-}$ Ion and Comparison with Time-Resolved X-ray and Spectroscopic Results

Irina V. Novozhilova, Anatoliy V. Volkov, and Philip Coppens*

Contribution from the Department of Chemistry, State University of New York at Buffalo, Buffalo, New York 14260-3000

Received July 25, 2002; E-mail: coppens@acsu.buffalo.edu

Abstract: A full understanding of the nature of excited states of transition metal complexes is important for understanding their chemical reactivity and role as intermediates in photochemically induced reactions. The ground and excited states of the $[\text{Pt}_2(\text{pop})_4]^{4-}$ ion are investigated using density functional theory (DFT). Calculations with different functionals employing quasi-relativistic Pauli and ZORA formalisms all predict a Pt–Pt bond shortening and a slight Pt–P lengthening upon excitation to the lowest triplet state, the latter in apparent contradiction to experimental EXAFS results. The PW86LYP functional with the ZORA relativistic treatment is found to produce good agreement with time-resolved crystallographic and spectroscopic results. A topological bond path between the Pt atoms is found in both the ground and the excited states, though the electron localization function (ELF) indicates weak Pt–Pt covalent bonding for the excited state only. The spin density is mainly localized on the Pt atoms, giving insight into the ability of the triplet excited state to abstract hydrogen and halogen atoms from organic substrates.

I. Introduction

Because of their chemical reactivity and role as intermediates in photochemically induced reactions and electron transfer, a full understanding of the nature of excited states of transition metal complexes is an important goal.¹ Computational methods are now sufficiently advanced to allow calculation of excited states of large molecular complexes. At the same time, the advent of time-resolved diffraction² is providing information that can serve as a test of computational methods and gives insight into the mechanism of photoinduced reactions.

The light-induced $^3\text{A}_{2u}$ excited state of tetrakis(pyrophosphito)diplatin(II) ($[\text{Pt}_2(\text{pop})_4]^{4-}$, pop = pyrophosphate, $(\text{H}_2\text{P}_2\text{O}_5)^{2-}$), or $[\text{HO}(\text{O})\text{POP}(\text{O})\text{OH}]^{2-}$, is highly reactive. It can abstract hydrogen atoms from a wide range of substrates, including alcohols, hydrocarbons, silanes and stannanes, as well as halogen atoms from alkyl and aryl halides, and effect both reductive and oxidative electron transfer.^{3,4} It acts as a photochemical dehydrogenation catalyst in the conversion of 2-propanol to acetone.⁵ The excited molecule can cleave duplex DNA by abstraction of both the 4'- and 5'-hydrogens from carbons of the 2'-deoxyribose groups.⁶

Spectroscopic analysis indicates a pronounced contraction of the metal–metal bond upon excitation, generally attributed to

a $5d\sigma^* \rightarrow 6p\sigma$ transition of an electron from a Pt–Pt antibonding orbital to an orbital which is bonding with regard to the Pt–Pt interaction. At room temperature, the $^3\text{A}_{2u}$ excited state has a lifetime of 9–10 μs in water and acetonitrile solutions, and a high quantum yield ($\phi_r = 0.5$ –0.6) for phosphorescence.⁷ As a result of spin–orbit coupling, the triplet level is split into two sublevels: a lower-lying A_{1u} level, and a second E_u level $\sim 42 \text{ cm}^{-1}$ higher in energy.⁸ As the A_{1u} level has a much longer lifetime than the E_u level, at ambient temperature, at which the spacing is much smaller than kT , the phosphorescence is mostly from the latter state, whereas at very low temperatures (below 30 K) the A_{1u} level with a lifetime of 6.06 ms⁸ dominates the emission process. As a result, the lifetime is strongly temperature dependent in the region in which the 42 cm^{-1} splitting is comparable with kT , a feature that can be used for temperature calibration purposes.¹¹

Recently, we have performed a first monochromatic time-resolved single-crystal diffraction experiment on the 50 μs (17 K) lifetime triplet excited state of the $[\text{Pt}_2(\text{pop})_4]^{4-}$ ion.¹⁰ The method is based on a stroboscopic pump–probe technique in

- (1) See for example: Vlček Jr., A. *Coord. Chem. Rev.* **2000**, 200–202, 933–977.
- (2) For an overview of recent progress see, *Faraday Discuss.* **2002**, 122.
- (3) (a) Vlček Jr., A.; Gray, H. B. *Inorg. Chem.* **1987**, 26, 1997–2000. (b) Roundhill, D. M.; Gray, H. B.; Che, C.-M. *Acc. Chem. Res.* **1989**, 22, 55–61. (c) Herman, M. S.; Goodman, J. L. *Inorg. Chem.* **1991**, 30, 1147–1149.
- (4) (a) Peterson, J. R.; Kalyanasundaram, K. *J. Phys. Chem.* **1985**, 89, 2486–2492. (b) Roundhill, D. M.; Shen, Z. P.; Atherton, S. J. *Inorg. Chem.* **1987**, 26, 3833–3835.
- (5) Harvey, E. L.; Stiegman, A. E.; Vlček Jr., A.; Gray, H. B. *J. Am. Chem. Soc.* **1987**, 109, 5233–5235.

- (6) (a) Kalsbeck, W. A.; Grover, N.; Thorp, H. H. *Angew. Chem., Int. Ed. Engl.* **1991**, 30, 1517–1518. (b) Kalsbeck, W. A.; Gingell, D. M.; Malinsky, J. E.; Thorp, H. H. *Inorg. Chem.* **1994**, 33, 3313–3316. (c) Carter, P. J.; Ciftan, S. A.; Sistare, M. F.; Thorp, H. H. *J. Chem. Educ.* **1997**, 74, 641–645. (d) Ciftan, S. A.; Thorp, H. H. *J. Am. Chem. Soc.* **1998**, 120, 9995–10000.
- (7) (a) Stiegman, A. E.; Rice, S. F.; Gray, H. B.; Miskowski, V. M. *Inorg. Chem.* **1987**, 26, 1112–1116. (b) Rice, S. F.; Gray, H. B. *J. Am. Chem. Soc.* **1983**, 105, 4571–4575.
- (8) Markert, J. T.; Clements, D. P.; Corson, M. R. *Chem. Phys. Lett.* **1983**, 97, 175–179.
- (9) Coppens, P.; Novozhilova, I. V. *Faraday Discuss.* **2002**, 122, 1–11.
- (10) Kim, C. D.; Pillet, S.; Wu, G.; Fullagar, W. K.; Coppens, P. *Acta Crystallogr. A* **2002**, 58, 133–137.
- (11) Ribaud, L.; Wu, G.; Zhang, Y.; Coppens, P. *J. Appl. Crystallogr.* **2001**, 34, 76–79.

Table 1. Ground State Geometries of $[\text{Pt}_2(\text{pop})_4]^{4-}$ Optimized with Different Density Functionals Using Pauli and ZORA Relativistic Methods (bond lengths in Å, Angles in deg)

	(TEA) ₃ H [Pt ₂ (pop) ₄] 17 K ^a	(TBA) ₂ H ₂ [Pt ₂ (pop) ₄] 90 K ^b	K ₂ [Pt ₂ (pop) ₄] 298 K ^c	B88P86			B88LYP			PW86LYP		
				Pauli FC	ZORA FC	ZORA AE _{Pt}	Pauli FC	ZORA FC	ZORA AE _{Pt}	Pauli FC	ZORA FC	ZORA AE _{Pt}
Pt–Pt	2.9126(2)	2.9238(16)	2.925(1)	2.837	2.948	2.979	2.859	2.969	3.000	2.972	3.039	3.072
Pt–P	2.3274(6)	2.3183(13)	2.320(5)	2.336	2.374	2.371	2.333	2.370	2.367	2.354	2.393	2.391
P–OH	1.5747(19)	1.579(3)	1.579(9)	1.618	1.644	1.645	1.607	1.633	1.633	1.624	1.651	1.651
P–O	1.5301(19)	1.517(3)	1.519(9)	1.540	1.561	1.561	1.524	1.545	1.545	1.527	1.548	1.548
P–O _b	1.6361(18)	1.620(3)	1.623(6)	1.672	1.702	1.702	1.656	1.686	1.686	1.670	1.700	1.700
∠PO _b P	128.12(10)	130.51(10)	133.3(9)	126.2	128.8	129.3	128.2	130.6	131.0	129.1	130.4	130.9

^a Kim, C. D.; Pillet, S.; Wu, G.; Fullagar, W. K.; Coppens, P. *Acta Crystallogr. A* **2002**, *58*, 133–137. ^b Kim, C. D. Ph.D. Thesis, State University of New York at Buffalo, 2002. ^c Che, C.-M.; Herbstein, F. H.; Schaefer, W. P.; Marsh, R. E.; Gray, H. B. *J. Am. Chem. Soc.* **1983**, *105*, 4604–4607.

which short X-ray probe pulses are synchronized with the pulses of an exciting laser beam. As the crystal is examined only during a short period immediately after excitation (33 μs in the $[\text{Pt}_2(\text{pop})_4]^{4-}$ experiment), the diffraction pattern is obtained during the short time span in which part of the molecules in the crystal are excited. The experiment is time-resolved in that the crystal is interrogated only during a very short time span during which a transient species exists, but this does not imply that a dynamic process has been followed at different points in time, as discussed elsewhere.⁹

We report here detailed density functional theory (DFT) calculations on the electronic structure and geometry of the ion in its ground and excited states, and the comparison of the theoretical results with both crystallographic and spectroscopic information.

II. Experimental Section

A. Ground-State Geometry. The structure of three different salts of the $[\text{Pt}_2(\text{pop})_4]^{4-}$ ion have been determined. Their structural parameters are listed in the first three columns of Table 1. The distances in (TEA)₃H[Pt₂(pop)₄], (TBA)₂H₂[Pt₂(pop)₄], and K₄[Pt₂(pop)₄]·2H₂O show a very small spread of ~0.01 Å, even though the solid-state environments are not the same, and the structure determinations were performed at different temperatures.

B. Time-Resolved Diffraction. Using stroboscopic diffraction with monochromatic synchrotron radiation, the geometry of the ³A_{2u} excited triplet state of the $[\text{Pt}_2(\text{pop})_4]^{4-}$ ion in a crystal of (TEA)₃H[Pt₂(pop)₄], (TEA=tetraethylammonium) was studied at 17 K.¹⁰ The pulsed-pump/pulsed-probe stroboscopic technique makes it possible to reach a time resolution much shorter than the read-out time of the detector, as the signal is only measured (repeatedly) during a very short time span immediately following excitation. The X-ray pulses are generated by a mechanical chopper, the synchrotron being used as an essentially continuous source, which is justified by the time scale of the experiment. The X-ray and laser pulses are synchronized, and thus occur with the same frequency. The frequency and X-ray pulse length to be selected in a particular study depend on the excited-state lifetime of the species to be examined. They were 5100 Hz and 33 μs, respectively, in the $[\text{Pt}_2(\text{pop})_4]^{4-}$ experiment, in accordance with the 50 μs lifetime of the excited state at the experimental temperature.

The analysis of the experimental observations is based on the light-induced intensity changes, which are combined with the intensities of the ground-state structure collected at the same temperature. The results indicate a shortening of the Pt–Pt bond upon excitation by 0.28(9) Å and a 3° molecular rotation of the excited molecules in the crystals.¹⁰ The experimentally determined change in geometry is illustrated in Figure 1.

C. Spectroscopic Information on Geometry Changes. The geometry of the ³A_{2u} excited state of the $[\text{Pt}_2(\text{pop})_4]^{4-}$ ion has been the subject of several spectroscopic studies. Franck–Condon analysis of

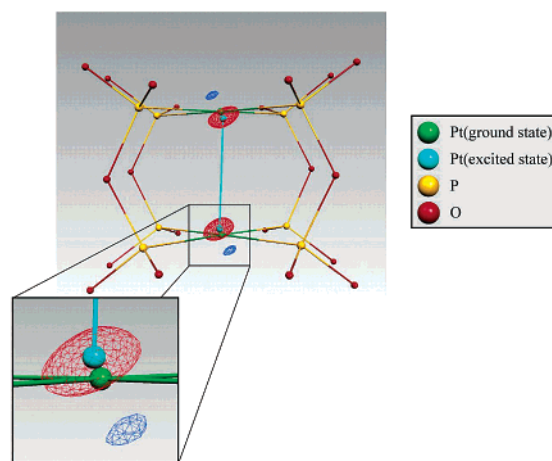


Figure 1. Three-dimensional photodifference map illustrating the difference between the electron densities after excitation and in the ‘dark’ crystal. A center of symmetry is located at the center of the drawing. Red areas positive, blue areas negative. Contours at $\pm 0.1 \text{ e}\text{\AA}^{-3}$.

the vibrational fine structure of the absorption and emission spectra of $[\text{Pt}_2(\text{pop})_4]^{4-}$ indicates a shortening of the Pt–Pt bond by 0.21 Å (with errors estimated at 10–15%), assuming that the metal–metal stretch involves only the Pt atoms.^{7b} This corresponds to a Pt–Pt excited-state bond length of 2.71 Å. Earlier work by Fordyce and Crosby gave, after correction for computational error, a shortening of 0.247 Å.^{7b,12} A study by Stein et al.¹³ based on Raman data and the empirical Badger’s rule, which relates a change in stretching frequency with a change in bond length, led to an excited-state bond length of 2.81 Å, corresponding to a shortening of only 0.10 Å. More recently, the geometry change associated with the ¹A_{2u}←¹A_{1g} (*dσ**→*pσ*) transition of (*n*-Bu₄N)₄[Pt₂(P₂O₅H₂)₄] was studied by Leung et al.,¹⁴ through an analysis of the resonance Raman intensities of an acetonitrile solution. On the basis of a simulation of the Raman intensities, a frequency shift of the Pt–Pt vibration from 115 cm⁻¹ to 177 cm⁻¹ was obtained, from which a bond length change of 0.225 Å was deduced, assuming harmonicity of the excited-state vibration. This result is in the same range as spectroscopic values quoted above for the singlet–triplet transition, and gives confidence in the methods employed in the various analyses.

D. EXAFS. An EXAFS study led to the conclusion that the distance between the two planes through the phosphorus atoms attached to each Pt atom is reduced by 0.52(13) Å upon excitation. However, because the sensitivity of the EXAFS spectrum to the long Pt–Pt bond is limited, a 2.75 Å Pt–Pt excited-state distance was assumed and combined with

- (12) Fordyce, W. A.; Brummer, J. G.; Crosby, G. A. *J. Am. Chem. Soc.* **1981**, *103*, 7061–7064.
 (13) Stein, P.; Dickson, M. K.; Roundhill, D. M. *J. Am. Chem. Soc.* **1983**, *105*, 3489–3494.
 (14) Leung, K. H.; Phillips, D. L.; Che, C.-M.; Miskowski, V. M. *J. Raman Spectrosc.* **1999**, *30*, 987–993.

Table 2. Lowest Singlet–Singlet and Singlet–Triplet Excitation Energies (in eV) from TD-DFT Calculations on the Ground-state Geometry Optimized with ZORA FC PW86LYP

$\Gamma_{C_{2h}}$	molecular orbital character	one-electron excitation	ΔE ZORA FC PW86LYP		exp. ^a	
			energy	oscillator strength	energy	oscillator strength
3A_u	HOMO→LUMO $d_{z^2}^* \rightarrow p_z$	$27a_u \rightarrow 32a_g$	2.82	0	2.74	0.000485
1A_u	HOMO→LUMO $d_{z^2}^* \rightarrow p_z$	$27a_u \rightarrow 32a_g$	3.48	0.1946	3.38	0.229
3B_u	HOMO-3,4→LUMO $p_{x,y}(L) \rightarrow p_z$	$32,31b_u \rightarrow 32a_g$	3.71	0		
3B_g	HOMO-1,2→LUMO $p_{x,y}(L) \rightarrow p_z$	$28,27b_g \rightarrow 32a_g$	3.74	0		
3A_u	HOMO→LUMO+1 $d_{z^2}^* \rightarrow d_{x^2-y^2}^*$	$27a_u \rightarrow 33a_g$	3.74	0		
1B_g	HOMO-1,2→LUMO $p_{x,y}(L) \rightarrow p_z$	$28,27b_g \rightarrow 32a_g$	3.83	0		
1B_u	HOMO-3,4→LUMO $p_{x,y}(L) \rightarrow p_z$	$32,31b_u \rightarrow 32a_g$	3.86	0.0073		
3A_g	HOMO→LUMO+1 $d_{z^2}^* \rightarrow d_{x^2-y^2}^*$	$27a_u \rightarrow 28a_u$	3.87	0		
1A_u	HOMO→LUMO+1 $d_{z^2}^* \rightarrow d_{x^2-y^2}^*$	$27a_u \rightarrow 33a_g$	3.87	0.17×10^{-6}		
1A_g	HOMO→LUMO+2 $d_{z^2}^* \rightarrow d_{x^2-y^2}^*$	$27a_u \rightarrow 28a_u$	4.03	0		

^a Shimizu, Y.; Tanaka, Y.; Azumi, T. *J. Phys. Chem.* **1984**, *88*, 2423–2425.

the other information from the spectrum.¹⁵ This distance was thus not independently determined. However, the Pt–P distances were directly measured and found to contract by 0.047(11) Å.

E. Spectroscopic Information on Energy Level Spacing. The low- and room-temperature measurements of the absorption spectrum of $[Pt_2(pop)_4]^{4-}$ have been performed in aqueous solutions and in single crystals containing different counterions.^{7,12,16} The recorded absorption spectra are similar in all cases, confirming that the dimeric geometry of $[Pt_2(pop)_4]^{4-}$ in the solid state is also preserved in the solution. The weak absorption at ~450 nm is attributed to the $^3A_{2u} \leftarrow ^1A_{1g}$ transition ($E_u(^3A_{2u})$ state), whereas the intense band at ~370 nm is associated with the $^1A_{2u} \leftarrow ^1A_{1g}$ transition ($^1A_{2u}$ state). The experimental excitation energies and the corresponding oscillator strengths are listed in Table 2.

III. Computational Details.

DFT calculations were carried out with the ADF2000.02¹⁷ suite of programs. The ground-state calculations were symmetry restricted to C_{2h} point group, whereas lower point group C_2 was used to optimize the excited state. Spin-restricted calculations were performed on the ground state (GS) structure, whereas for the excited triplet state (ES_{tr}) unrestricted open-shell calculations were done. Several exchange-correlation density functionals were used in the geometry optimization. Because the Local Density Approximation (LDA) with the functional of Vosko–Wilk–Nusair (VWN5)¹⁸ did not reproduce the ground-state geometry satisfactorily, the Generalized Gradient Approximation (GGA) was applied. The valence atomic orbitals of platinum, oxygen, phosphorus, and hydrogen atoms were described by triple- ζ Slater-type basis sets with one polarization function added on the O, P, and H atoms (ADF database IV). The (1s2s2p)¹⁰ and (1s)² shells of P and O, respectively, were treated by the frozen core (FC) approximation in all calculations.¹⁹ The (1s2s2p3s3p4s3d4p4d)⁴⁶ core shells of Pt were either kept frozen or all electrons of Pt were used in the computation in which case the core was described by double- ζ quality basis set (in

the following the Pt all-electron calculations are labeled as AE_{Pt}). Relativistic effects were taken into account using either of two methods implemented in ADF: a quasi-relativistic method which employs the Pauli Hamiltonian,²⁰ and the zero order regular approximation (ZO-RA).²¹ Due to the variational instability of the Pauli Hamiltonian, the quasi-relativistic Pauli method can only be applied with the frozen-core approximation. The ZORA method is variationally stable and can be used in all-electron calculations. Geometry convergence was considered reached when the Cartesian gradients were below 10^{-4} Hartree/Å. All of the optimized molecular geometries were confirmed as true energy minima by the positive eigenvalues of the Hessian matrixes. Time-dependent density functional theory (TD-DFT)²² calculations were performed on the equilibrium ground-state geometries of the $[Pt_2(pop)_4]^{4-}$ anion employing the same density functionals and basis sets used in geometry optimization. The Davidson algorithm was used, in which the error tolerance in the square of the excitation energies and trial-vector orthonormality criterion were set to 10^{-8} and 10^{-10} , respectively. The success of TD-DFT method in calculating excitation energies of transition metal complexes has been demonstrated in several recent studies.²³ The program MOLDEN 3.7 was used for visualization of the orbitals.²⁴ The ADF output data were converted to MOLDEN format with ADF2MOLDEN.²⁵ 3D representations of the spin and deformation densities were prepared with MOLEKEL4.1.²⁶

- (15) Thiel, D. J.; Liviš, P.; Stern, E. A.; Lewis, A. *Nature* **1993**, *362*, 40–43.
 (16) Shimizu, Y.; Tanaka, Y.; Azumi, T. *J. Phys. Chem.* **1984**, *88*, 2423–2425.
 (17) (a) Baerends, E. J.; Ellis, D. E.; Ros, P. *Chem. Phys.* **1973**, *2*, 41–51. (b) Versluis, L.; Ziegler, T. *J. Chem. Phys.* **1988**, *88*, 322–328. (c) te Velde, G.; Baerends, E. J. *J. Comput. Phys.* **1992**, *99*, 84–98. (d) Fonseca Guerra, C.; Snijders, J. G.; te Velde, G.; Baerends, E. J. *Theor. Chem. Acc.* **1998**, *99*, 391–403.
 (18) Vosko, S. H.; Wilk, L.; Nusair, M. *Can. J. Phys.* **1980**, *58*, 1200–1211.
 (19) Baerends, E. J.; Ellis, D. E.; Ros, P. *Chem. Phys.* **1973**, *2*, 41–51.

- (20) (a) Boerrigter, P. M.; Baerends, E. J.; Snijders, J. G. *Chem. Phys.* **1988**, *122*, 357–374. (b) Ziegler, T.; Tschinke, V.; Baerends, E. J.; Snijders, J. G.; Ravenek, W. *J. Phys. Chem.* **1989**, *93*, 3050–3056.
 (21) (a) Chang, C.; Pelissier, M.; Durand, M. *Phys. Scr.* **1986**, *34*, 394–404. (b) van Lenthe, E.; Baerends, E. J.; Snijders, J. G. *J. Chem. Phys.* **1993**, *99*, 4597–4610. (c) van Lenthe, E.; Baerends, E. J.; Snijders, J. G. *J. Chem. Phys.* **1994**, *101*, 9783–9792. (d) van Lenthe, E.; van Leeuwen, R.; Baerends, E. J.; Snijders, J. G. *Int. J. Quantum Chem.* **1996**, *57*, 281–293.
 (22) (a) van Gisbergen, S.; Kootstra, F.; Schipper, P. R. T.; Gritsenko, O. V.; Snijders, J. G.; Baerends, E. J. *Phys. Rev. A* **1998**, *57*, 2556–2571. (b) Jamorski, C.; Casida, M. E.; Salahub, D. R. *J. Chem. Phys.* **1996**, *104*, 5134–5147. (c) Bauernschmitt, R.; Ahlrichs, R. *Chem. Phys. Lett.* **1996**, *256*, 454–464.
 (23) (a) van Gisbergen, S. J. A.; Groeneveld, J. A.; Rosa, A.; Snijders, J. G.; Baerends, E. J. *J. Phys. Chem. A* **1999**, *103*, 6835–6844. (b) Rosa, A.; Baerends, E. J.; van Gisbergen, S. J. A.; van Lenthe, E.; Groeneveld, J. A.; Snijders, J. G. *J. Am. Chem. Soc.* **1999**, *121*, 10 356–10 365. (c) Boulet, P.; Chermette, H.; Daul, C.; Gilardoni, F.; Rogemond, F.; Weber, J.; Zuber, G. *J. Phys. Chem. A* **2001**, *105*, 885–894.
 (24) Schaftenaar, G.; Noordik, J. H. *J. Comput.-Aided Mol. Design* **2000**, *14*, 123–134.
 (25) Volkov, A. V. Program ADF2MOLDEN, State University of New York at Buffalo, 1999.

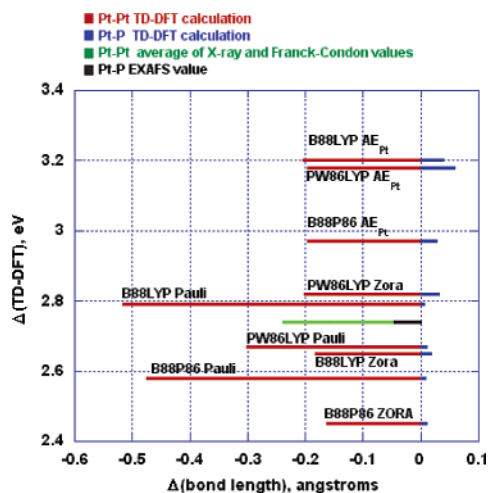


Figure 2. Summary of theoretical and experimental results for Pt–Pt and Pt–P bond changes upon $^3(d\sigma^* \rightarrow p\sigma)$ excitation, and TD-DFT and experimental excitation energies. The Δ SCF values for the energy difference between relaxed ground and excited states do not differ appreciably from the plotted TD-DFT values (Table S1 of the Supporting Information).

IV. Theoretical Results and Comparison with Experiment.

A. Geometries of the Ground State and Excited Triplet State of $[\text{Pt}_2(\text{pop})_4]^{4-}$. **1. Ground State.** The calculated geometrical parameters of the ground state of the $[\text{Pt}_2(\text{pop})_4]^{4-}$ ion are listed in Table 1, together with experimental results from one room-temperature and two low-temperature X-ray structure analyses.^{10,27} The largest Pt–Pt distances are from the all-electron calculations, which lengthen the Pt–Pt bond by 0.03 Å compared with the frozen-core treatment. The Pt–Pt bond is also very sensitive to the type of relativistic treatment used, the ZORA values being as much as 0.08 Å longer than those obtained with the Pauli Hamiltonian. As may be expected, the bridging angles $\angle\text{PO}_b\text{P}$ change in parallel with the Pt–Pt bond lengths, a shorter Pt–Pt distance corresponding to a smaller value of the angle. A strong dependence on the type of calculation is also evident for the Pt–P bond, whereas the P–O, P–OH and P–O_b bond lengths are much less affected.

Though in solid $(\text{TEA})_3\text{H}[\text{Pt}_2(\text{pop})_4]$ and $(\text{TBA})_2\text{H}_2[\text{Pt}_2(\text{pop})_4]$, the $[\text{Pt}_2(\text{pop})_4]^{4-}$ anions form one-dimensional chains held together by intermolecular hydrogen bonds, the effect on the geometry of $[\text{Pt}_2(\text{pop})_4]^{4-}$ is small, as bond lengths differ little from those in solid $\text{K}_4[\text{Pt}_2(\text{pop})_4] \cdot 2\text{H}_2\text{O}$, in which the anions are isolated from each other by the K^+ ions.²⁸ The variation between the experimental results for the three structures is much smaller than the spread among the different theoretical values.

2. Excited Triplet State. The results of geometry optimization of the excited triplet state using B88P86, B88LYP, and PW86LYP density functionals are given in Table S1 and, for Pt–Pt and Pt–P bonds, graphically summarized in Figure 2. As is the case for the ground-state Pt–Pt bond length, the magnitude of its shortening upon excitation is very much dependent on both the density functional selected and on the relativistic method employed. The B88LYP and B88P86 functionals with Pauli FC predict the largest reduction of the Pt–Pt

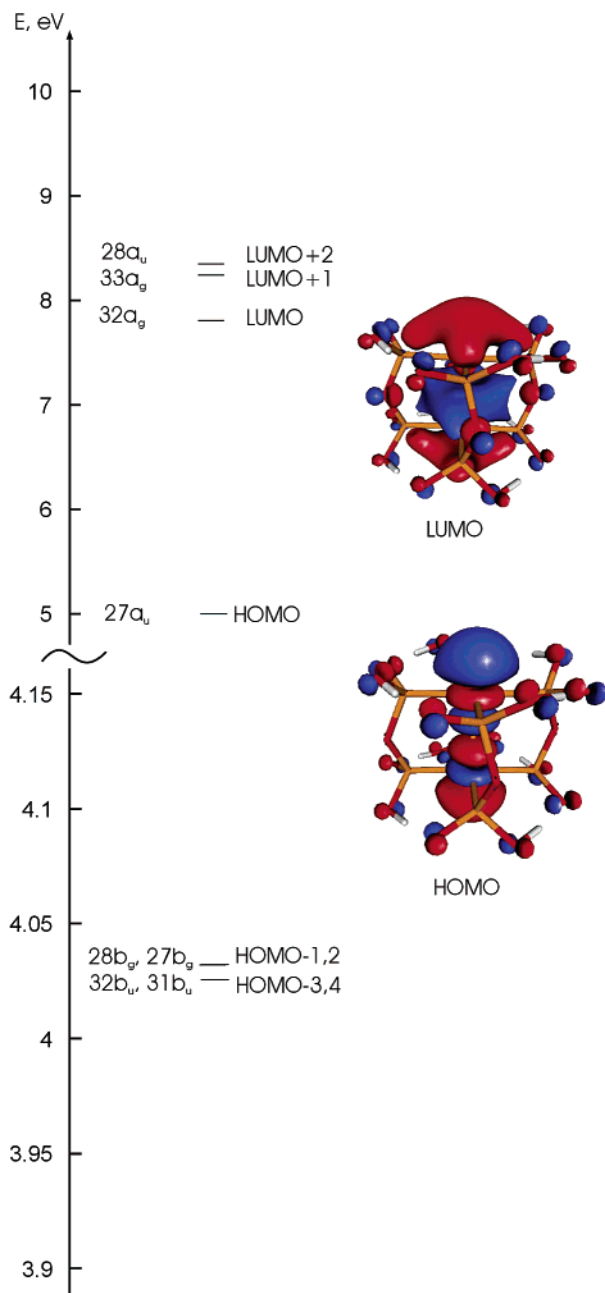


Figure 3. Ordering of the frontier molecular orbitals in the ground state. Isosurface value 0.025 au.

bond upon excitation ($\Delta \approx -0.5$ Å). Replacement of the Pauli with the ZORA Hamiltonian consistently reduces the shortening. The Pt–P bond length is invariably calculated to be larger in the excited state; the strengthening of the Pt–Pt interaction being accompanied by a weakening of the other bonds to Pt. This result contradicts the interpretation of the EXAFS spectra.

As FC PW86LYP results for both the Pt–Pt shortening and the 3A_u TD-DFT excitation energy agree well with the experimental information, this method is used here in the discussion of ground-state and 3A_u excited-state properties of the $[\text{Pt}_2(\text{pop})_4]^{4-}$ ion.

B. Molecular-Orbital Analysis. Notwithstanding the different predictions for the bond lengths, all DFT methods give the same ordering of the orbitals and topologically identical orbital surfaces. The relative energies of the frontier molecular orbitals, and the equi-probability surfaces of the HOMO and LUMO

(26) *Molekel4.1*, Flükiger, P.; Lüthi, H. P.; Portmann, S.; Weber, J., Swiss Center for Scientific Computing, Manno, Switzerland, 2000–2001.

(27) Kim, C. D. Ph.D. Thesis, State University of New York at Buffalo, 2002.

(28) Dos Remedios Pinto, M. A. F.; Sadler, P. J.; Neidle, S.; Sanderson, M. R.; Subbiah, A.; Kuroda, R. *J. Chem. Soc., Chem. Commun.* **1980**, 13–15.

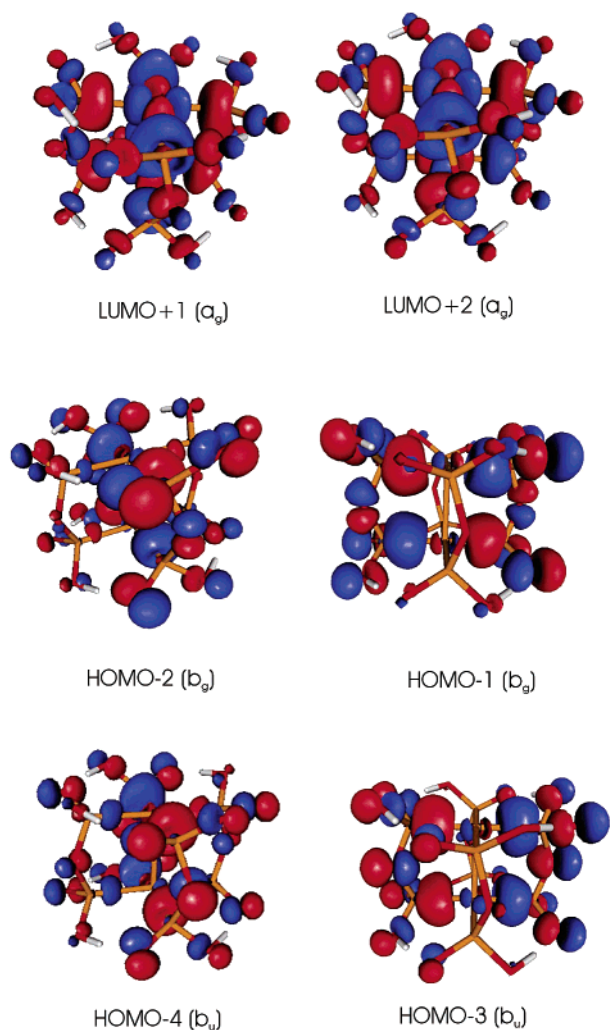


Figure 4. Equi-probability surfaces of the ground-state molecular orbitals just above and below the HOMO–LUMO levels. Isosurface value 0.03 au.

levels, as calculated with the ZORA FC PW86LYP method, are plotted in Figure 3. The HOMO level is d_{z^2} -metal like in character and antibonding in the Pt–Pt region, whereas the LUMO has major contributions from the p_z atomic orbitals on the Pt atoms and is bonding in this region, thus confirming the accepted interpretation of the Pt–Pt bond shortening as due to an antibonding to weakly bonding transition. The other occupied frontier orbitals are mainly localized on the P and O atoms (Figure 4), whereas the vacant LUMO+1 and LUMO+2 levels have significant Pt $d_{x^2-y^2}$ contributions. The ordering of the orbitals in the excited-state remains the same as in the ground state (Figure 5).

C. Excitation Energies. The TD-DFT approach provides an alternative to computationally demanding multireference configuration interaction methods in the study of excited-states.²⁹ This method is especially attractive for large systems for which the cost of the correlated ab initio methods may be prohibitive.

(29) see for example (a) Fabian, J. *Theor. Chem. Acc.* **2001**, *106*, 199–217. (b) Andreu, R.; Garin, J.; Orduna, J. *Tetrahedron* **2001**, *57*, 7883–7892. (c) Petiau, M.; Fabian, J. *THEOCHEM* **2001**, *538*, 253–260. (d) Boulet, P.; Chermette, H.; Daul, C.; Gilardoni, F.; Rogemond, F.; Weber, J.; Zuber, G. *J. Phys. Chem. A* **2001**, *105*, 885–894. (e) Hsu, C.-P.; Hirata, S.; Head-Gordon, M. *J. Phys. Chem. A* **2001**, *105*, 451–458. (f) Van Gisbergen, S. J. A.; Guerra, C. F.; Baerends, E. J. *J. Comput. Chem.* **2000**, *21*, 1511–1523. (g) Wakamatsu, K.; Nishimoto, K.; Shibahara, T. *Inorg. Chem. Commun.* **2000**, *3*, 677–679.

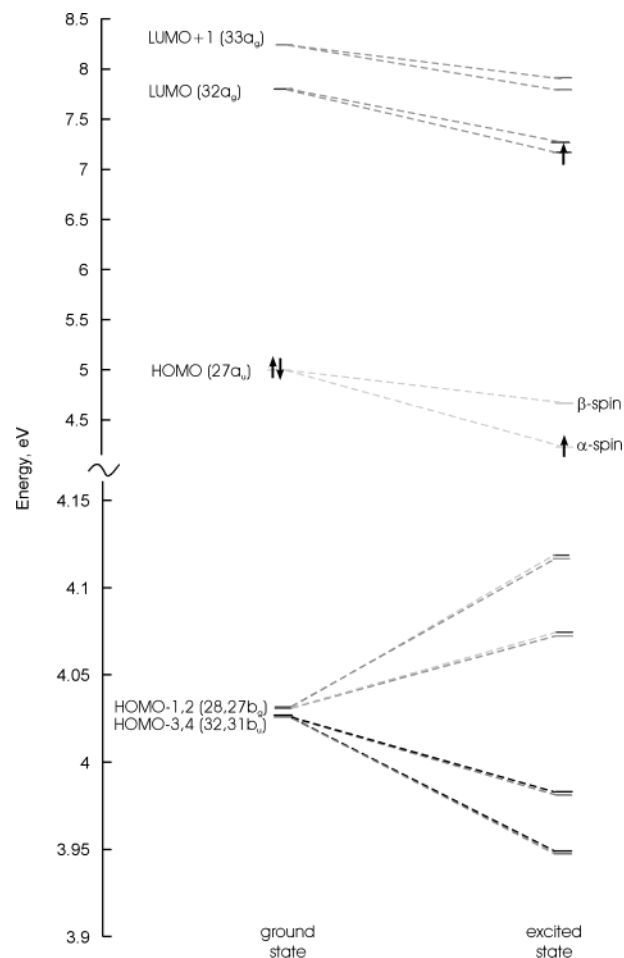


Figure 5. Energy levels of the molecular orbitals just above and below the HOMO–LUMO level in the ground state and excited triplet state according to ZORA FC PW86LYP calculation. In the description of the orbitals C_{2h} symmetry notation is used. The arrows indicate the electron population of the highest occupied orbitals in each case.

The results for the first excitation energies calculated with the PW86LYP method are compared with the experimental values in Table 2. As the TD-DFT calculations do not evaluate the spin–orbit splitting, the values are averaged over the E_u and A_{1u} states into which the triplet level is split. (A separate spin–orbit configuration interaction (SO–CI) calculation with the program GAMESS–US, not further reported here, did quantitatively reproduce the 42 cm^{-1} splitting of the triplet level.) The lowest calculated singlet and triplet excitations correspond to the transition from HOMO to LUMO. The results of the calculations are in good agreement with the reported experimental values for the low-energy transitions (1A_u and 3A_u states), as is the calculated oscillator strength f of the singlet–singlet transition.

The higher-lying excitations in the calculated absorption spectrum correspond to weak metal d–d and ligand-to-metal charge-transfer transitions. Additional calculations with the Pauli quasi-relativistic treatment, not reported here, indicate the effect of the nature of the relativistic treatment to be as large as 0.5 eV for several of the excitations.

D. Energy Decomposition of the Ground and Excited States. According to the transition state method of Ziegler and Rauk,³⁰ the bonding energy ΔE of a molecular system can be written as the sum of three physically significant terms: $\Delta E =$

Table 3. Decomposition of the Total Bonding Energy (in eV) in the Ground and Excited Triplet States from ZORA FC PW86LYP Calculation

energy terms	GS	ES _{tr}	Δ
Pauli repulsion, ΔE _{Pauli}	752.41	744.85	-7.56
electrostatic, ΔE _{el}	-237.07	-234.31	+2.76
orbital total, ΔE _{orb}	-750.51	-742.89	+7.62
total bonding	-235.17	-232.36	+2.81

Table 4. Hirshfeld Charges for the Ground State and Excited Triplet State from ZORA FC PW86LYP Calculation

atom	GS	ES _{tr}	Δ(ES _{tr} - GS)
Pt	0.053	0.115	+0.062
P	0.326	0.313	-0.013
O _b	-0.283	-0.285	-0.002
O	-0.419	-0.418	+0.001
O _H	-0.339	-0.340	-0.001
H	0.060	0.059	-0.001

Table 5. Mulliken Atomic Spin Population (in electrons) for the Excited Triplet State of [Pt₂(pop)₄]⁴⁻ from ZORA FC PW86LYP Calculation

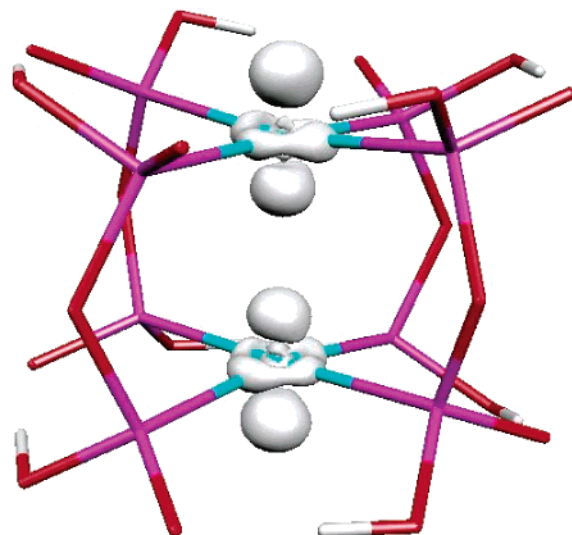
atom	spin population	atom	spin population
Pt	0.604	O	0.017
P	0.062	O _H	0.012
O _b	0.010	H	0.003

$\Delta E_{el} + \Delta E_{Pauli} + \Delta E_{orb}$, ΔE_{el} is classical electrostatic interaction between the unperturbed charge distributions of the fragments or atoms in which the molecule is partitioned, ΔE_{Pauli} comprises electron–electron destabilizing interactions between occupied orbitals on the fragments and accounts for the steric repulsion, whereas the orbital interaction ΔE_{orb} corresponds to interactions among occupied and virtual orbitals on two fragments. ΔE_{orb} accounts for formation of electron pair bonds, charge transfer and polarization (empty/occupied orbital mixing).

Results of the analysis with the PW86LYP functional are listed in Table 3. The decrease in Pauli repulsion ΔE_{Pauli} by -7.56 eV upon excitation of [Pt₂(pop)₄]⁴⁻ can be related to the lengthening of all but Pt–Pt bonds. At the same time, the electrostatic interaction ΔE_{el} becomes less attractive, and the orbital interaction ΔE_{orb} less favorable, leading to a total destabilization of 2.81 eV (Table 3). The Hirshfeld³¹ charges (Table 4) indicate a change of charge on the platinum atom from +0.053e in the ground state to +0.115e in the triplet state. The charges on all other atoms in the molecule are affected by no more than ~0.01e (Table 4).

E. Unpaired Spin Density of the Triplet State. The spin populations of the excited state are summarized in Table 5. 60% of the spin population is localized on the Pt atoms (Figure 6). The high spin density on the Pt atoms may be related to the ability of the triplet excited state to abstract hydrogen and halogen atoms from organic substrates.^{3b}

F. Topological Analysis of the Charge Density. Topological analysis of the total electron density is increasingly used to characterize the nature of metal–metal bonding. It is now recognized that the distinction between open-shell and closed shell interactions based on $\nabla^2\rho(\mathbf{r})$ at the bond critical point,

**Figure 6.** 3D representation of the spin density ('spin up' minus 'spin down') of the excited triplet state of [Pt₂(pop)₄]⁴⁻. Plotted isosurface contour 0.01 au.

while proven useful for bonding between first row atoms, is not sufficient when heavier atoms are involved.³² For metal atoms the valence density tends to be diffuse and the electron density at the bcp relatively small, which means that its second derivatives are not well determined. Other features, including the total energy density $H(\mathbf{r})$ and the kinetic energy density $G(\mathbf{r})$ at the bcp and the ratio of these quantities to $\rho(\mathbf{r}_c)$ are better preserved when descending in the periodic table. For an open shell interaction the negative potential energy density $V(\mathbf{r}_c)$ outweighs the positive kinetic energy density to give a negative value of $H(\mathbf{r}_c)$, with $G(\mathbf{r}_c)/\rho(\mathbf{r}_c)$ typically <1, but >1 for closed shell interactions.^{33,34}

Results for the Pt–Pt bond, obtained with the program XAIM³⁵ are presented in Table 6. Even in the ground state a bond path links the two Pt atoms (Figure 7). For both states the bond critical point (bcp) is characterized by small values of the total density $\rho_c(\mathbf{r})$ and positive value of Laplacian $\nabla^2\rho_c$. The potential energy density at the bcp is negative in both cases, but more so in the excited state, leading to a more negative value of $H(\mathbf{r}_c)$, even though the kinetic energy density also increases. The more negative values of both $H(\mathbf{r}_c)$ and $H(\mathbf{r}_c)/\rho_c$ in the excited state are in agreement with the increase in ρ_c , also evident in the deformation densities for the two states (Figure 8), and with the increased bonding character of the excited state. In the ground state, the kinetic energy density divided by the electron density at the bcp, $G(\mathbf{r})/\rho_c$ in the Pt–Pt bond is <1, as generally expected for covalent bonds; it is somewhat larger in the excited triplet state $G(\mathbf{r})/\rho_c$ but still <1. All changes are in the opposite direction for the Pt–P bonds, which lengthen on excitation.

Further insight in the nature of the bonding is provided by the ELF function, introduced by Becke and Edgecombe,³⁶ and developed further by Savin and Silvi.³⁷ It is defined as $\eta(\mathbf{r}) = [1 + (D(\mathbf{r})/D_h(\mathbf{r}))^2]^{-1}$, where $D(\mathbf{r})$ and $D_h(\mathbf{r})$ are related to the

(30) (a) Ziegler, T.; Rauk, A. *Inorg. Chem.* **1979**, *18*, 1558–1565. (b) Ziegler, T.; Rauk, A. *Inorg. Chem.* **1979**, *18*, 1755–1759. (c) Ziegler, T.; Rauk, A. *Theor. Chim. Acta* **1977**, *46*, 1–10.

(31) Hirshfeld, F. L. *Theor. Chim. Acta* **1977**, *44*, 129–138.

(32) Cremer, D.; Kraka, E. *Croat. Chem. Acta* **1984**, *57*, 1259–1281.

(33) Macchi, P.; Garlaschelli, L.; Martinengo, S.; Sironi, A. *J. Am. Chem. Soc.* **1999**, *121*, 10 428–10 429.

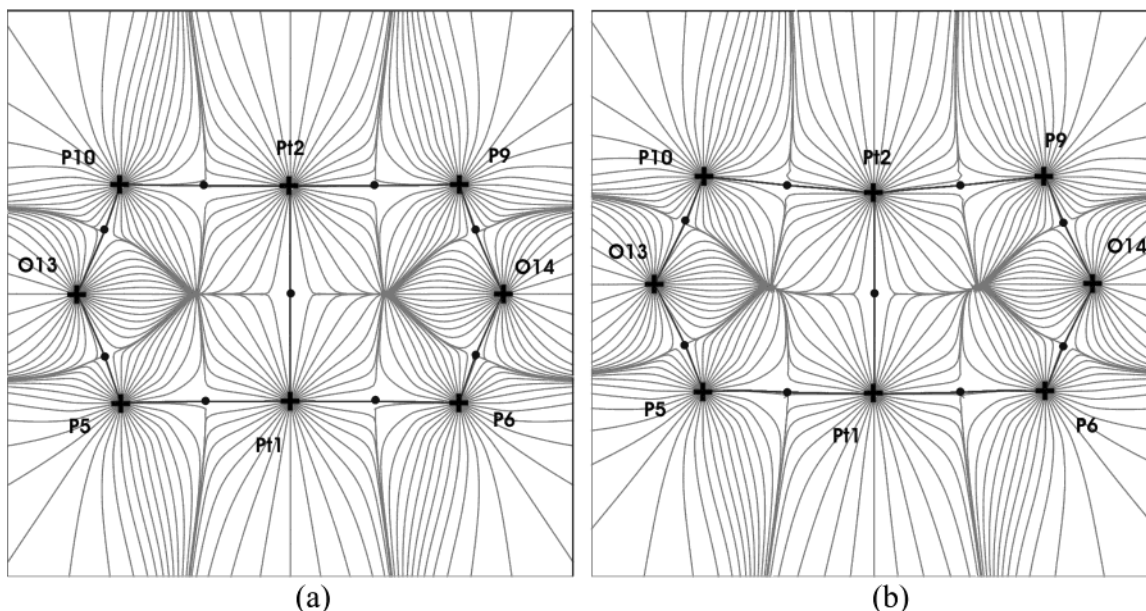
(34) Macchi, P.; Sironi, A., *Coord. Chem. Rev.*, in press.

(35) *Xaim-1.0*, Ortiz Alba, J. C.; Bo, C. Universitat Rovira I Virgili, Tarragona, Spain. <http://www.quimica.urv.es/XAIM>

Table 6. Topological Properties (in a.u.) at the Pt–Pt and Pt–P Bond Critical Points of the Ground State (first line) and the Excited Triplet State (second line) of $[\text{Pt}_2(\text{pop})_4]^{4-}$ complex (ZORA FC PW86LYP calculation)

	ρ_c	λ_1	λ_2	λ_3	$\nabla^2\rho_c$	e	$V(\mathbf{r}_c)$	$G(\mathbf{r}_c)$	$G(\mathbf{r}_c)/\rho_c$	$H(\mathbf{r}_c)$	$H(\mathbf{r}_c)/\rho_c$
Pt–Pt	0.035	−0.024	−0.024	+0.080	+0.033	0	−0.016	0.012	0.343	−0.004	−0.114
	0.051	−0.037	−0.037	+0.122	+0.048	0	−0.032	0.022	0.431	−0.010	−0.196
Pt–P	0.100	−0.086	−0.083	+0.382	+0.213	0.025	−0.127	0.090	0.900	−0.037	−0.370
	0.095	−0.080	−0.078	+0.355	+0.197	0.022	−0.117	0.083	0.874	−0.034	−0.358

^a ρ_c – total charge density at the bcp. ^b $\nabla^2\rho_c$ – Laplacian of charge density at the bcp. ^c $\lambda_1, \lambda_2, \lambda_3$ – eigenvalues of $\nabla^2\rho_c$ ($\nabla^2\rho_c = \lambda_1 + \lambda_2 + \lambda_3$). ^d e – bond ellipticity. ^e $G(\mathbf{r}_c)$ – electronic kinetic energy density at the bcp. ^f $V(\mathbf{r}_c)$ – electronic potential energy density at the bcp. ^g $H(\mathbf{r}_c)$ – the total electronic energy density ($H(\mathbf{r}_c) = G(\mathbf{r}_c) + V(\mathbf{r}_c)$).

**Figure 7.** Trajectories of the gradient of the charge density in the plane defined by Pt1, Pt2, and P6 for the ground state (a) and excited triplet state (b). The bond paths are indicated by solid lines, the bond critical points are denoted by filled circles. The graphs were generated with locally modified version of TOPXD (Volkov, A.; Abramov, Y.; Coppens, P.; Gatti, C. *Acta Crystallogr. A* **2000**, *56*, 332–339).

electron pair probability density for same spin electrons for the system of interest, and for the homogeneous electron gas with the similar spin density, respectively. ELF values vary from 0 to 1, the upper limit corresponding to perfect electron-pair localization. The reference value of 0.5 corresponds to electron-pair density in homogeneous gas. Because ELF is directly related to the electron pair probability density, its graphic representation can contribute to a qualitative understanding of electron localization.

The ELF isosurfaces for the ground state of $[\text{Pt}_2(\text{pop})_4]^{4-}$, calculated with the program of Autschbach and Ziegler³⁸ and visualized with MOLEKEL²⁶ are presented in Figure 9. At $\eta(\mathbf{r}) = 0.658$ (Figure 9a) the valence domains $V(\text{P}–\text{O})$, $V(\text{P}–\text{O}_\text{H})$, and $V(\text{O}–\text{H})$ can be identified. The $V(\text{P}–\text{O})$, $V(\text{P}–\text{O}_\text{H})$, and $V(\text{O}–\text{H})$ domains are cylindrical and demonstrate the bonding interaction typical for single bonds. At $\eta(\mathbf{r}) = 0.815$ the bonding between P and O atoms in $[\text{Pt}_2(\text{pop})_4]^{4-}$ resembles that calculated for the H_3PO molecule, in which the P–O bond was described as having both polarized covalent and ionic character.³⁹ At $\eta(\mathbf{r}) = 0.815$, a localization domain is visible between platinum and phosphorus, located close to the latter atom. The nature of ELF for the Pt–P bond supports its interpretation as a polar covalent bond with dative ligand-to-metal character.⁴⁰

Even though the topological parameters of the ground-state Pt–Pt suggest an open-shell interaction, no $V(\text{Pt}–\text{Pt})$ domain is evident from the plotted ELF. At $\eta(\mathbf{r}) = 0.658$ two types of platinum monosynaptic basins can be identified: the core basin $C(\text{Pt})$ enclosed by a very compact nonbonding valence basin $V(\text{Pt})$, which is fragmented at the value of the contour used in the figure (Figure 9a). Similar metal valence ELF domains were found for $\text{Fe}_2(\text{CO})_9$ and $\text{Rh}_6(\text{CO})_{16}$.⁴¹

The ELF isosurface at $\eta(\mathbf{r}) = 0.815$ in the excited triplet state resembles the ELF of the ground state and therefore is not presented here. However, lower values of $\eta(\mathbf{r}) = 0.28–0.33$ give additional information (Figure 9b). The small disk on the Pt–Pt axis, approximately at its midpoint, can be interpreted as Pt–Pt electron pairing. The Pt–Pt pairing region is observed at a rather small ELF value and is very compact, similar to the Ti–Co interaction in $(\text{H}_2\text{N})_3\text{Ti}–\text{Co}(\text{CO})_3(\text{PH}_3)$,⁴² in which the small value of the ELF for the metal–metal bonding ($\eta_{\text{Ti}–\text{Co}} = 0.42$) is attributed to the low contribution of d orbitals with high angular momentum quantum numbers to ELF.⁴³

V. Summary and Conclusions

The experimental information on the excitation energy and geometry changes upon excitation of the title compound are

(36) Becke, A. D.; Edgecombe, K. E. *J. Chem. Phys.* **1990**, *92*, 5397–5403.
 (37) Silvi, B.; Savin, A. *Nature* **1994**, *371*, 683–686.
 (38) Program *ELF*, Autschbach, J.; Ziegler, T. The University of Calgary, Canada, 2000.
 (39) Chestnut, D. B. *Heteroatom Chem.* **2000**, *11*, 341–352.

(40) Jansen, G.; Schubart, M.; Findeis, B.; Gade, L. H.; Scowen, I. J.; McPartlin, M. *J. Am. Chem. Soc.* **1998**, *120*, 7239–7251.
 (41) Kaupp, M. *Chem. Ber.* **1996**, *129*, 527–533.
 (42) Jansen, G.; Schubart, M.; Findeis, B.; Gade, L. H.; Scowen, I. J.; McPartlin, M.; *J. Am. Chem. Soc.* **1998**, *120*, 7239–7251.
 (43) Kohout, M.; Savin, A. *J. Comp. Chem.* **1997**, *18*, 1431–1439.

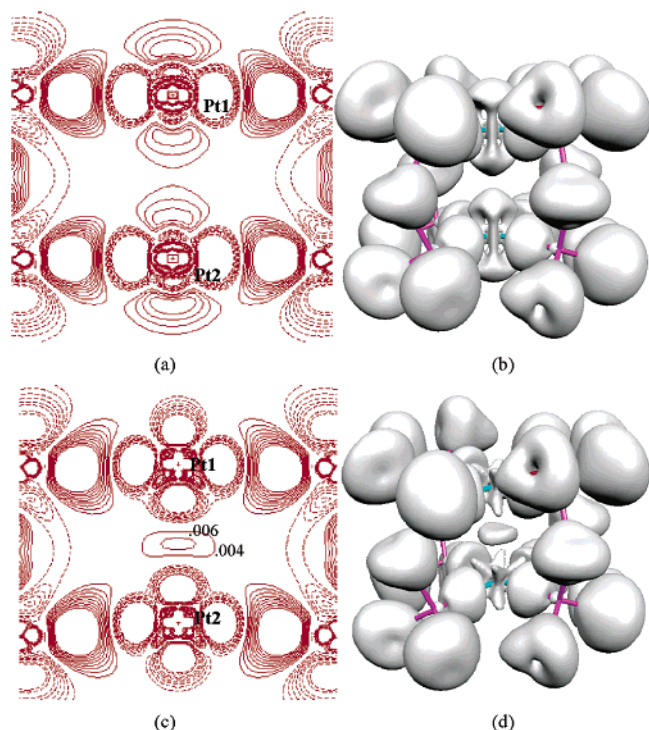


Figure 8. Theoretical deformation density maps of the ground state (a), (b) and excited state (c), (d) of $[\text{Pt}_2(\text{pop})_4]^{4-}$. (a) and (c) 2D maps in the plane containing Pt1, Pt2 and a phosphorus atom. Contour intervals at 0.002 au; positive levels solid lines, zero contour omitted. (b) and (d) 3D-view of the theoretical deformation density. Isosurface value 0.004 au. Only positive density is shown.

qualitatively reproduced by all DFT functionals applied in this work. All calculations predict a Pt–Pt bond shortening and a slight Pt–P lengthening upon excitation to the lowest triplet state. Good agreement is obtained with the PW86LYP functional combined with the ZORA relativistic treatment, except for the Pt–P bond length change as determined by EXAFS, which is at variance with all theoretical studies and must therefore be regarded with caution.

Topological analysis of the ground and excited state electron densities from the ZORA FC PW88LYP calculation reveals a bond path connecting the Pt atoms in both the ground and excited states, with the total energy density and the kinetic energy density per electron at the BCP, though small, being negative and <1 respectively as found for open shell interactions. However, the ELF of the *ground* state does not support electron pairing in the Pt–Pt region. The *excited*-state ELF does show the formation of electron pairing between the metal atoms, although at a rather low ELF value.

Finally, we want to emphasize that the experimental results on the structure of short-lived species, which are now becoming available, must be combined with parallel theoretical calculations such as presented here if a comprehensive understanding of the nature of transient species and their role in chemical processes is to be attained.

Acknowledgment. Financial support of this work by the National Science Foundation (CHE9981864) and the Petroleum Research Fund of the American Chemical Society (PRF32638AC3) is gratefully acknowledged. The computations were performed on the 64-processor SGI Origin3800, 32-processor Sun Blade 1000 (UltraSparc III) and 48-processor Sun Ultra-5 (UltraSparc

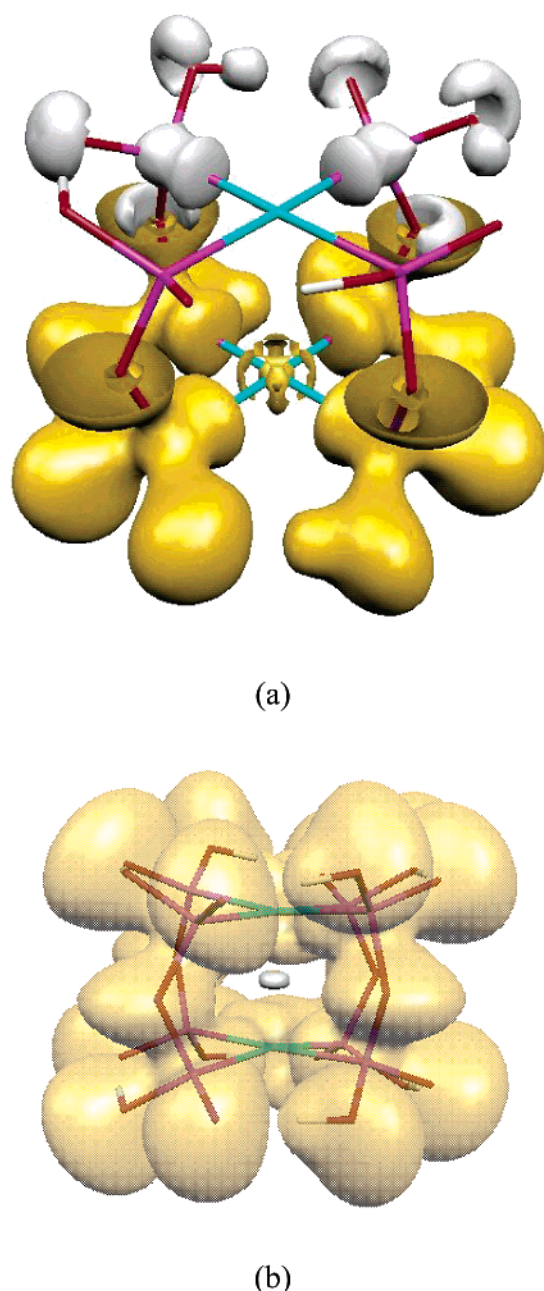


Figure 9. Theoretical electron localization function (ELF) of $[\text{Pt}_2(\text{pop})_4]^{4-}$ at isovalues 0.815 (gray) and 0.658 (yellow) for the ground state (a), and at 0.30 for the excited state (b). For clarity in (a) the two surfaces are shown separately in the upper and lower part of the drawing, while in (b) the platinum–platinum electron pairing region is colored in solid gray and all other regions of ELF are shown in transparent yellow.

III) supercomputers at the Center for Computational Research of the State University of New York at Buffalo which is supported by grant (DBI9871132) from the National Science Foundation. Research carried out in part at the National Synchrotron Light Source at Brookhaven National Laboratory, which is supported by the U.S. Department of Energy, Division of Materials Sciences and Division of Chemical Sciences. The Ar^+ laser used in the diffraction experiments was provided under Grant No. CHE0087817 to Chem/Met CARS, administered by the University of Chicago. The authors would like to thank Dr. Jochen Autschbach (Prof. Tom Ziegler's group, University of Calgary) for providing a copy of the ELF program, Dr. José

Carlos Ortiz Alba and Carles Bo Jané (Universitat Rovira I Virgili) for the Xaim program, and Dr. Sebastien Pillet for the drawing of Figure 1.

Supporting Information Available: Table S1 containing optimized triplet state geometries, and Δ SCF and TD-DFT triplet

excitation energies calculated with different density functionals employing Pauli and ZORA relativistic methods and frozen-core and all-electron basis set on Pt. This material is available free of charge via the Internet at <http://pubs.acs.org>.

JA027857B